ELSEVIER

Microelectronic Engineering 27 (1995) 427-434

MICROELECTRONIC ENGINEERING

Phase Grating Masks for Photonic Integrated Circuits Fabricated by E-Beam Writing and Dry Etching: Challenges to Commercial Applications

D.M. Tennant, K. Feder, K. F. Dreyer, R.P. Gnall, T.L. Koch, U. Koren, B.I. Miller, and M.G. Young

AT&T Bell Laboratories
Holmdel, New Jersey, USA 07733

Near field holography is a method of using grating photomasks in which the m = -1 and m = 0 diffracted beams of a UV source interfere to form a standing wave pattern. This simple hologram can then be used to expose a grating pattern on a process wafer when held in near- contact. This technique is especially attractive for use in OEICs and PICs when fabrication of the grating masks is accomplished with e-beam lithography and dry etching, since the diffractive properties of the mask can be controlled by the physical parameters of the mask. The grating period on masks made in this way can be precisely controlled to produce arrays of lasers each separated by only a small change in frequency (order 100 GHz) as may be required for WDM applications. We review the phenomenology of fused silica phase grating masks and describe work toward establishing characterization criteria, implementing practical printing methods, improving e-beam precision, and demonstrating laser array performance. We discuss principle issues and progress in each of the technical areas.

1. INTRODUCTION

Future broad band lightwave communications will require continued advances in optoelectronic integrated circuits (OEICs) and photonic integrated circuits (PICs) to provide economical solutions to system manufacture. System designs which employ wavelength division multiplexing (WDM) architecture will likely require semiconductor laser arrays to provide multi-wavelength light sources integrated with other optical components such as combiners, modulators, etc. Practical processing methods are therefore needed to influence the introduction of this technology in timely fashion. One such opportunity lies in the production of corrugated-waveguide gratings which are key elements for many of the optical devices such as filters and distributed feedback (DFB) or distributed Bragg reflector (DBR) lasers that are expected to play an important role in PICs. The challenge is to produce an array of gratings closely spaced with precise features in an economically viable way. Conventional two-beam UV laser holographic methods are not well suited to manufacture of laser arrays where pitch variations in adjacent channels and abrupt shifts within the gratings are needed. While such structures have been demonstrated using e-beam direct-write-on-wafer [1,2], a parallel printing technique is preferred to avoid the slow serial writing process. In our work we have studied and developed near field holographic (NFH) printing using pure phase masks as an alternative method of producing grating structures.

In this printing technique UV light is incident on a grating mask at an angle θ_i from the normal. The beam is partially transmitted (zero order) and partially diffracted (first order). These two beams then function just as in the conventional two-beam interference method, causing a periodic intensity variation below the mask at the spatial period of the grating. This intensity pattern is used to expose photoresist that subsequently is developed and used as an etch mask for wet chemical or dry etching of a corrugated grating in the semiconductor.

NFH printing of first order gratings using phase+amplitude polymer replica gratings [3] and fused silica phase grating masks [4-6] have been demonstrated to be an alternative method of printing grating structures for semiconductor lasers [3,5-7]. Direct write e-beam [5,7] lithography is a flexible way to generate these masks and to include systematic pitch changes needed for WDM applications. Using high resolution e-beam tools, pitch adjustment increments as fine as 0.0039 nm and abrupt phase shifts can be made within a single mask.

Challenges to commercial implementation of this method are still formidable. The issues include acceptance of WDM technology as a terrestrial platform for lightwave communication and the continued improvement of NFH as a robust and economical method. While the former will be decided in the marketplace, we continue

Elsevier Science B.V.
SSDI 0167-9317(94)00139-1

to make progress toward the latter. In this article we review the principles and characterization methods of NFH and then address technological issues which impact the economical use of the method.

2. THEORY

For light at wavelength λ incident on a grating mask at an angle θ_i we have $k_{x0} = 2\pi/\lambda \sin\theta_i$. The grating with pitch Λ_g produces diffracted orders m with the k_x values $k_{xm}=k_{x0}+2\pi m/\Lambda_g$. For the grating pitches studied here in the range of Λ_g~240 nm, and illumination at a wavelength of λ~ 364 nm, we find that indeed only the m=0 and m=-1 orders satisfy $|k_{xm}|< 2\pi/\lambda$ as required for non-evanescent propagation after the mask. In fact, to generate any diffracted wave that propagates after the mask requires that $\sin\theta_i > \lambda/\Lambda_g$ -1, or for our work, $\theta_i>31^o$.

To predict the effects of the various physical parameters on the diffractive properties an analytical model would be desirable. The simple approach using scalar diffraction theory assumes the field just after the mask is the incident field multiplied locally by a spatially-varying phase retardation. This "phase plate" is evaluated simply by propagating the incident field in each region ignoring diffractive effects during the propagation through the mask itself. This theory predicts, however, that the most power that can be diffracted into the first order is 40.5% [4] and that equal power is diffracted into the m =+1 order, which is not even a propagating wave. The simple scalar diffraction theory also predicts power diffracted into other higher orders which are also evanescent. This treatment also lacks polarization dependence. The flaw in the scalar theory is that it ignores diffractive effects going through the mask, which is inadequate when the grating features become comparable to the incident wavelength. In the case here, each grating tooth is only a third of the optical wavelength, therefore a more rigorous diffraction theory is required.

Diffraction from phase gratings of arbitrary pitch and profile has been formulated in a rigorous manner by Moharam and Gaylord[8]. Their treatment makes full use of the Maxwell equations including proper treatment of boundary conditions and reflected waves. While the general cyclic behavior of the diffracted intensity and undiffracted intensity is qualitatively similar to the scalar theory, the rigorous treatments show that nearly 100% of the power can be diffracted into the first order for a proper depth. Also, the rigorous theory properly indicates that indeed the only waves leaving the sample are the specular and first-order diffracted reflections, and the undiffracted and first-order diffracted transmitted beams.

As an example, Fig 1 plots the ratio of the first order diffracted to zero order transmitted power , R_d, as function of etch depth calculated by Moharam from the rigorous theory [9] for a square wave phase grating with a period, Λ = 240 nm. The plot assumes an index of refraction, n=1.5, a duty cycle, f=0.5, an illumination angle, θ_i=48.6 deg by λ=360 nm TE polarized radiation. The theory predicts increasing power into the diffracted (m=-1) beam and decreasing power in the zero order with groove depth, resulting in a monotonically increasing value of the ratio R_d as seen in the figure. Since the phenomenon is cyclical, this trend continues to a depth of about 0.45 μm then reverses (not shown). The optimum point is of course R_d=1 which corresponds under these conditions to an etch depth of about 0.23 μm. The case for a square wave is not general, however, and the specific values of the maximum R_d and the reversal point depend in detail on the tooth shape and symmetry [8].

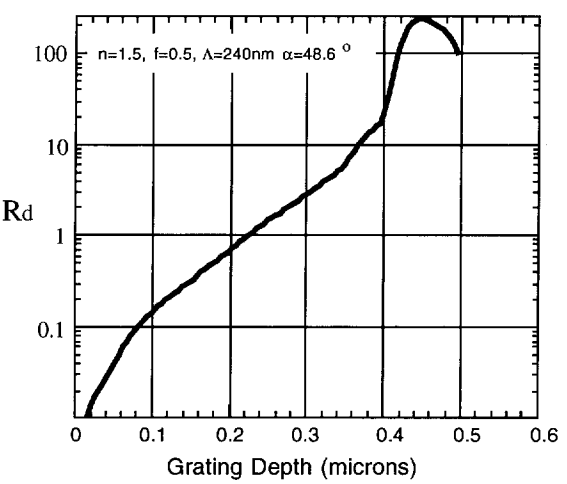

FIG. 1 Calculated ratio of the first order diffracted power to the transmitted power as a function of etch depth (Adapted from data supplied by M.G. Moharam, Ref 9)

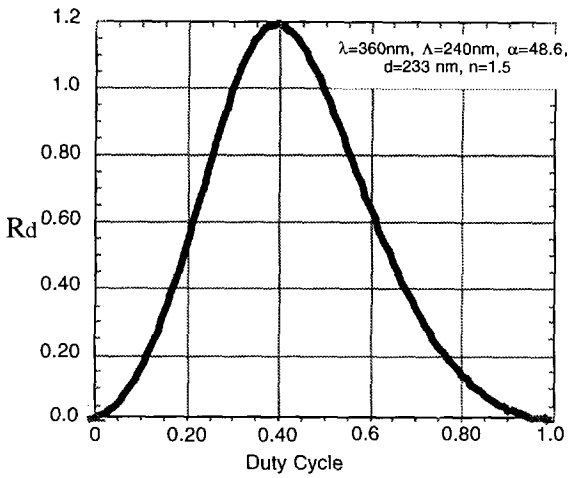

FIG. 2 Calculated ratio of the first order diffracted power to the transmitted power as a function of duty cycle (Adapted from data supplied by M.G. Moharam, Ref 9)

Fig 2 plots R_d for varying duty cycle assuming a fixed etch depth of 233nm and otherwise identical conditions. We note that R_d is somewhat sensitive to the duty cycle and that it is not peaked at 50%. The peak is actually skewed slightly to just below 40%.

Our experimental evidence of the dependence of R_d on etch depth and duty cycle deviate somewhat from these predictions for the structures we have fabricated. This will be discussed below.

3. GRATING MASK FABRICATION AND CHARACTERIZATION

The extremely fine changes in period required for wavelength division multiplexing for light wave communications cannot be achieved using straightforward means of encoded patterns of various periods. This approach can suffer from discretization minima in the address structure. In our approach we make use of a fine gain adjustment made to the e-beam system while using a coded 250 nm period grating pattern. Under normal operation this adjustment is used to correct the e-beam system metrology during the writing session, but it can also be used to intentionally stretch or shrink each axis. The DAC setting in our system permits 12-bits of correction to an adjustment range of 6.4% of the maximum field size, thus allowing 0.0039 nm changes in the grating period for the 250 nm pattern. The minimum adjustment varies linearly, of course, with the period of the coded pattern. Since the overall gains in x and y are adjusted, any phase shifting section of the grating is expanded or shrunk by the same relative amount. Therefore a Λ/2 (l/4) phase shift initially coded into the grating pattern remains the same fraction of the period even after adjustment.

We have adopted a two level lithography process to produce the actual square-wave phase masks. Our starting substrate is a commercially available chromium coated fused silica photomask blank. In the first step we define the regions of the blank in which the chromium is to be opened by UV photolithography and wet chemical etching. The first level typically includes: windows for gratings at each device site; fiducial marks which indicate cleave positions; e-beam alignment marks; and windows for etch depth monitors and other process monitors.

The square wave pure phase gratings are fabricated essentially as previously reported [5]. The gratings are patterned using e-beam lithography in a tri-layer resist process. The gratings for this work were contained within a single writing field in order to avoid field stitching errors within the area spanned by individual devices.

More reliable performance and smoother gratings were obtained using a PMMA imaging layer, however, and was therefore used for masks in which the total writing area was small. For larger areas, we have had good results using ZEP 320 as our imaging resist [7], which substantially reduces the writing times. The grating pattern is written in the opened windows but overlapped a small amount with the chromium at the edge. After development the pattern is transferred into the thin Ge and hard baked photoresist by RIE using CF_3Br and O_2, respectively. The resulting pattern is etched into the fused silica using RIE in CHF_3. The etch mask is then removed in an oxygen RIE. Generally, linewidths are not preserved during the process, especially since the CHF_3 etch step can deposit polymer on the sidewalls of the etch mask while removing material from the bottom of the grooves in the fused silica.

The principal parameters needed to characterize a grating mask are the grating pitch accuracy and the diffraction efficiency. The period of the gratings are determined by precisely

measuring the first order diffraction angle. The sample is mounted on a rotation stage and illuminated with an Argon ion laser (λ= 363.8 nm). The beam incident on the grating results in a specularly reflected beam, a transmitted beam, a forward diffracted beam and a backward diffracted beam. The sample is first oriented to specularly retro-reflect the incident beam. The sample is then rotated to align the backwards first-order diffracted beam to retro-reflect upon the incident beam path. The difference in angle between these two positions(49.28 degrees for the Λ= 240 nm gratings) determines the period of the grating by simple geometry:

$$\Lambda_g = \lambda / 2 \sin\theta_i$$

In our earlier work, gratings fabricated in ten different test lots yielded a mean deviation from the design period of 0.05% [4]. Since our simple angular measurement was limited to a resolution of 2 minutes of arc, this value appears measurement-limited. For the period increment measurements, a stepper motor controlled rotation stage allowed more precise measurements of the pitch changes. The minimum angle increment of the stepper motor is 0.01 degrees which corresponds to a grating pitch change of 0.0189 nm.

Using a similar experimental arrangement we have measured the power in the transmitted and forward diffracted beams. A lens is inserted between the incident TE-polarized beam and the mask in order to focus the entire laser beam within the grating area. The power into the zero and first order (transmitted) diffracted beams are sequentially measured using a detector large enough to fully capture each beam. Masks with the highest contrast in the image are obtained when the power into the zero and first order beams are equal. If we define C as the ratio of the intensities at the maxima and minima in the image, then,

$$C = [(\sqrt{R_d}+1) / (\sqrt{R_d}-1)]^2 .$$

As stated R_d (and therefore C) of the fused silica grating mask is dependent on the etched depth, duty cycle, and tooth shape [4,8]. For all the gratings reported here, a standard groove depth of 220- 250 nm was maintained. The duty cycle is therefore the principal variant in determining the diffraction efficiency. Our previous study confirmed the Moharam analysis [9] in that the best balance between the diffracted (first order) and undiffracted (zero order) beams are not obtained for 50% duty cycle. Rather a duty cycle (given by tooth width (l) to period Λ ratio) of about 1/3 is optimum. To approach a 33% duty cycle in the fused silica grating, the initial lithography is biased to narrower developed openings (40%) to compensate for a general widening of the grooves as the various RIE steps are completed. A scanning electron micrograph (SEM) of a representative cross section of the grating is shown in Fig. 3. We observe that while the profiles are not perfect, they are nearly a square wave profile. Earlier experiments in which etch depth was varied for a constant duty cycle indicated a discrepancy with the theory. We observe a peak rather than the expected continuous increase in the diffracted (m=-1) power with deeper etching [4]. The small differences from ideal, both in the profile of the grating and the duty cycle along the grooves may account for some of the departure from the theoretical depth dependence of R_d.

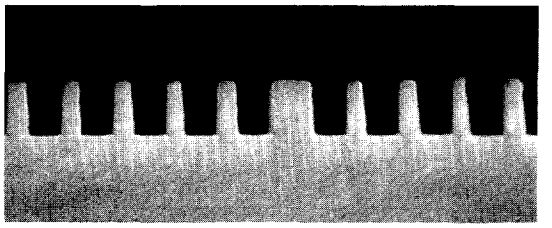

FIG. 3 Cross sectional view SEMs of the completed phase grating in fused silica

With these target parameters we have fabricated and characterized a variety of grating masks for DBR and DFB laser arrays. An 8-wave DBR laser array mask layout comprised 960 gratings with eight periods in increments of 0.127 nm. The minimum design grating period was 242.861 nm and the maximum was 243.750 nm. The measured value of Λ for the maximum period was 243.87 nm, within our experimental uncertainty for the absolute period setup. The average change in period, $\Delta\Lambda$, given by the slope of a linear fit to the data, was 0.131 nm. This mask was used to produce DBR laser arrays previously reported [5].

Another DBR mask design comprising 16 different grating types with similar design increments was made . The layout for this laser array groups the different gratings more closely (250 μm on center) while spacing consecutive

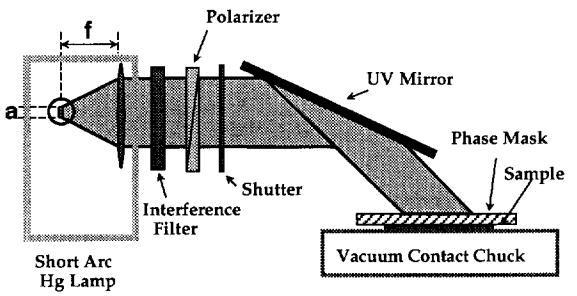

FIG. 4 Schematic of the modified contact aligner used to print NFH gratings.

groups more sparsely to allow for other system components. The mean period is 243.63 nm, again within the measurement error of the design period of 243.7 nm, and the average pitch change is 0.126 nm (the goal was 0.127 nm). The beam power ratio for all the gratings on both this and the previous mask fell between 0.49 and 0.91. Most of this variation is due to intentional changes in the dose of the e-beam write which results in small duty cycle variations. This range in power ratios results in a range of intensity variations, C, in the interference patterns of from 1760 to 32, -more than adequate to produce good contrast in the printing process.

Quarter-wave shifted DFB are even more challenging since typical DFB laser designs require longer, more closely spaced gratings with precise pitch control and a precise $\Lambda/2$ phase shifting section. DFB laser array results from our most recent NFH mask are described below.

4. GRATINGS FOR DFB LASERS USING A COMMERCIAL EXPOSURE TOOL

We have installed and evaluated a commercially available UV contact mask aligner which was modified to allow NFH printing. The platform for the system is a Karl Suss Model MJB3 contact mask aligner with the light source and condenser optics removed. Since the near field use of the gratings described requires only local spatial coherence and limited temporal coherence from the source, a conventional short arc mercury lamp can be used. We calculate that for a commercially available lamp with a 0.25 mm arc using an f=50 mm condenser optic and an interference filter centered at 365 nm, good fringe visibility requires a gap between the phase mask and wafer of only 12 μm or less [10]. The lamp housing, a polarizing filter, collimating lens, 365 nm chromatic filter, and shutter are mounted along with the aligner on a small optical table. A schematic of the NFH aligner is shown in Fig 4. The collimated light enters the rear of the Suss aligner where it is then reflected onto the mask at an illumination angle of about 45 degrees via a modified UV mirror mount in the mask aligner. The aligner also contains the wafer translation and rotation adjustment and the vacuum contact wafer chuck.

Figure 5a is a tapping mode atomic force microscope (AFM) image of an e-beam generated fused silica grating mask. Figure 5b is an AFM

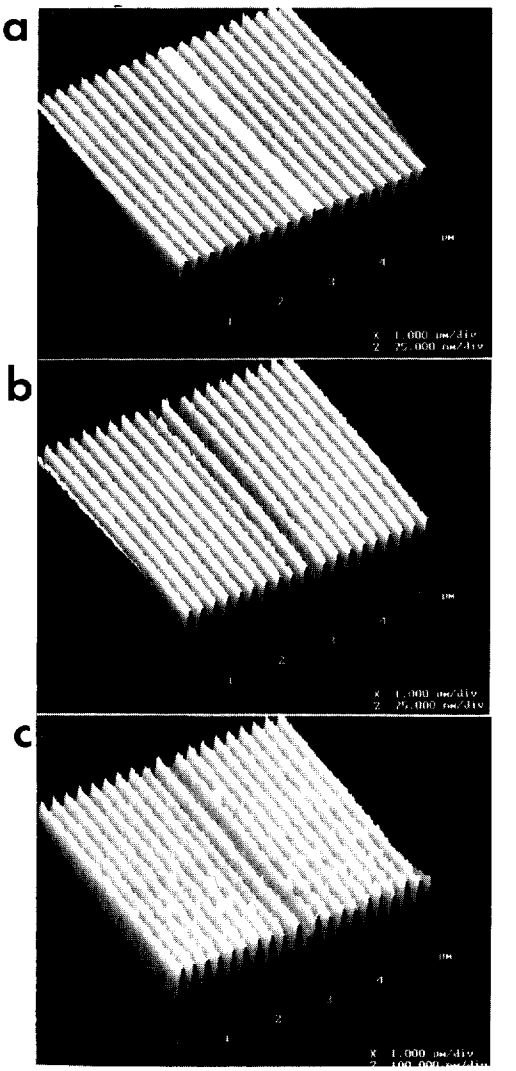

FIG. 5 Tapping mode atomic force microscope images of a $\lambda/4$ shifted-type grating a) for an e-beam written fused silica mask b) printed in resist on an InP wafer , and c) chemically etched into an InP wafer.

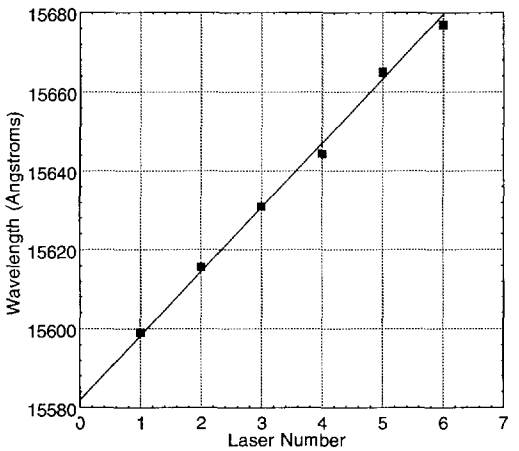

FIG. 6 Plot of the emission peaks of a 1X6 λ/4 shifted DFB laser array

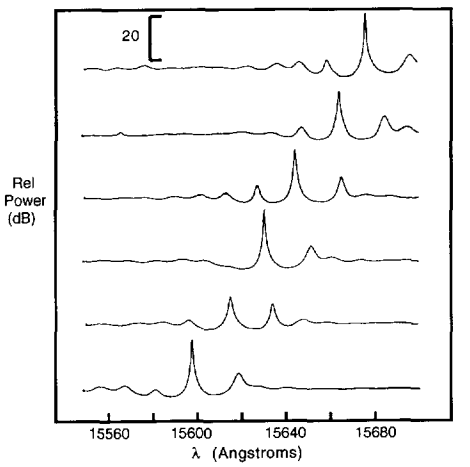

FIG. 7 Spectral Response of a 1X6 λ/4 shifted DFB laser array

image of a grating printed on a resist coated InP wafer using such a mask in the Suss aligner. The photoresist layer was spin coated to a thickness of 50nm and pre-baked in air. The wafer was exposed at a nominal dose of 40 mJ/cm2 and developed in Shipley developer. Exposures are performed by aligning the grating grooves with the TE polarization direction. A long postbake is used to improve resist adhesion before transfer of the grating by chemical etching in a bromine-based etchant. The AFM images of the resultant grating is shown in Fig 5c. We observe from Fig 5 that the abrupt phase shift in the original mask blurs only slightly in the resist and also after a subsequent chemical etch of the InP as seen in the middle and bottom images, respectively. The contact obtained in the Suss aligner using our 0.060 inch thick mask plates is more than adequate to provide good quality printing. We noted that there can be difficulty for some combinations of mask and wafer types. For example when 0.020 inch thick fused silica grating masks were used, we found that there could be significant bowing of the mask, especially when the wafers were small, non-beveled, square samples. This results in poor contact, with gaps even greater than the coherence length of our source. These pitfalls are easily avoided if rigid masks blanks are used.

Masks similar to that depicted in Fig 5a made by our standard e-beam lithography and dry etching method were designed to produce 1 X 6 arrays of DFB lasers. The six laser channels are separated in frequency by 200 GHz and as close as 80 μm spatially. The 200 GHz corresponds to about a 0.28 nm grating pitch change per channel. This trial included designs for lasers with single abrupt λ/4 (Λ/2) shifted gratings.

The lasers used in this experiment were standard semi-insulating planar buried heterostructure design [11,12] employing MQW active layers. In the particular example here, the gratings were fabricated by reactive ion etching a corrugation entirely though a thin 1.3μm bandgap InGaAsP layer above the active layer, followed by the mesa formation and regrowth of the lateral current blocking layers and the upper InP cladding layers. Hence the grating teeth consist of buried InGaAsP islands. In our case, the laser length was 380μm with an array repeat distance of 508 μm. Figure 6 shows the measured peak wavelengths of a bar of six lasers. The average frequency spacing was approximately 193.5 GHz, close to the design value of 200 GHz. The line in the figure is the best fit to a 200 GHz channel spacing. A bar of these lasers was mounted with AR coatings applied to both facets. Figure 7 shows the emission spectrum of all six devices driven below threshold clearly indicating the characteristic dominant longitudinal mode centered in the DFB stop-band as expected with a λ/4 shifted design.

5. PRACTICAL ISSUES

Large single period grating masks may also be of interest in producing DFB and DBR lasers which do not require varying periods. This process is usually accomplished by grating definition using interfering UV laser holography. To demonstrate adaptation of NFH to printing of large

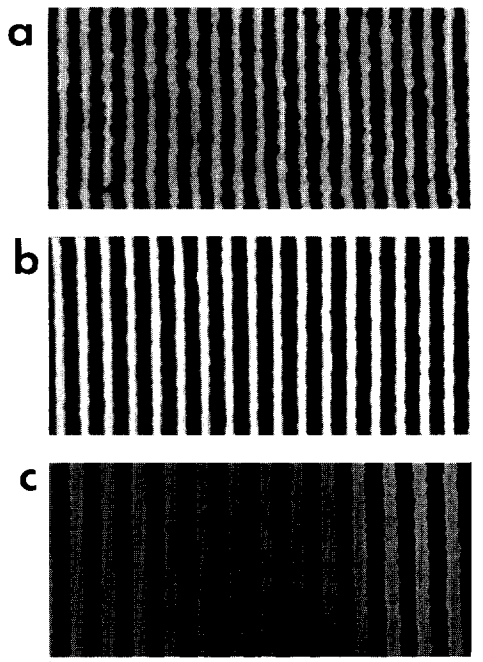

FIG. 8 Scanning electron micrographs of three large area fixed period phase grating masks with periods of a) 200 nm b) 240 nm c) 300 nm.

area gratings, we fabricated phase grating masks with Λ = 200, 240, and 300 nm prepared by UV laser split-beam corner-cube holographic exposure using the 363.8 nm ultraviolet line of an argon ion laser. The grating masks are formed over about a three inch diameter area using a trilayer resist comprising a lower layer of hard baked photoresist and a middle layer of germanium, similar to the e-beam trilayer but with a UV photoresist top layer. The exposed top layer is wet developed, followed by reactive ion etching of the lower layers and fused silica grating grooves to a depth of 0.24 μm. Figure 8 shows SEMs of three completed masks with different periods gratings. The power ratio, R_d, is in the range 1.0 to 0.59 for all wavelengths, comparable to that of e-beam generated masks. AFM images of the developed resist printed using the large area mask are quite good although edge roughness is coarser than in the e-beam case.

We studied the effects of extended contact printing on the grating masks and the resulting print quality. In general agreement with Pakulski, et. al.. [6] we observe that about 20 to 30 wafer prints can be performed without significant change in the quality of the printed gratings. Higher numbers of prints often showed signs of increased defects, however. [7] The typical failure mode results from significant debris accumulation after repeated exposures. While we have been somewhat successful cleaning these masks, some portion of the damage can be permanent

To extend the utility of the e-beam generated masks we successfully made second generation mask copies by NFH. Use of mask copies with shifted gratings (e.g., DFB laser masks) will cause the phase shifting region printed on the wafer to be broadened twice. The spatial extent of the $\lambda/4$ shifting region in a typical print from an e-beam mask is about 1.25 μm. Further broadening to 2 or 3 μm after printing from a copy is not expected to noticeably affect the grating performance for DFB lasers.

This copy process was also conducted for the holographically produced gratings. From SEMs of several copies made in this way, we judge them to be sub-par compared to that of the e-beam generated masks. Both edge roughness in the original mask and difficulty in obtaining vacuum contact due to the poor seal between the aligner gasket and the grating grooves contributed to this result in our judgment.

In general, the second generation e-beam masks are of sufficient quality to suggest that in high volume production that the original mask might only be used to create copies which are, in turn, used on the shop floor.

Another issue which impacts both the quality and economics of this technology is the throughput for e-beam written masks. Grating masks can require exceedingly long direct write times even when gratings are written only in selected areas. In part this is due to the desire to use both a conservative beam diameter and a high resolution, high contrast resist in order to improve process latitude. In a similar vein, uniformity improves with good depth of focus and low distortion. And, although not a strict requirement [13], best results are obtained when no field stitching is used to complete each laser grating site. These requirements generally imply using a small convergence angle in the electron optical column in order to achieve uniform writing over large areas. This results in a low current density beam. For our current system, a JEOL JBX 5DII which employs a CeB_6 thermionic cathode, operated at 50 kV a typical current density is about 25 A/cm2. Laser array masks for 2 inch wafer processing contain grating areas of about 30 mm^2. Areal writing rates for gratings using PMMA resist are about 0.42 mm^2/hr which

translates into three days of writing. Switching from PMMA to a more sensitive resist is an important step. We chose ZEP 320 due to its demonstrated high resolution [14] , good contrast, reasonable etch resistance, and simple development process. The immediate improvement in throughput from the resist can be about a factor of 6.5, reducing the same write to about 11 hours. A second major potential improvement can be realized by using a higher brightness electron source, such as a Zr/W thermal field emitter (TFE), which can provide substantially higher current densities (1000 - 2000 A/cm2). This can result in an additional factor of 40 in writing speed if the maximum deflection speed of the e-beam system is not reached.

6. CONCLUSIONS

Near field holographic printing appears to be a viable method of printing grating structures for WDM applications. It combines the flexibility of direct write e-beam lithography with the throughput of UV contact photolithography. Pitch control in our initial trials appears to be better than 0.1 nm for periods near 0.24 μm. This corresponds to about a 0.7 nm uncertainty in the lasing wavelength.

Both duty cycle and the groove depth in the fused silica phase masks are important parameters for obtaining nearly balanced diffracted and undiffracted beams --the condition desired for maximum printing contrast. Our approach has been to use a pure phase grating and fixed illumination angle while optimizing the grating by varying the depth and duty cycle. The adaptation of a commercially available contact mask aligner has proven to be a straightforward method of implementing the NFH technique for wafer scale applications.

The various laser array masks discussed illustrate good quality linearity in the channel spacing. The 1X16 and 1X8-wavelength DBR laser array mask with 100 GHz channel spacing are offered as examples. Our latest 1X6 DFB laser array fabricated with the NFH process exhibited excellent wavelength control with emission spectra clearly characteristic of a λ/4-shifted DFB design.

To further leverage the effort expended in making a high quality mask, we found that each master mask could be used to generate multiple second generation masks which preserve the period and abrupt phase shifts such as are required for DFB laser arrays.

By using more sensitive resists and high brightness sources, writing times for current masks can be reduced by over a factor of one hundred. This should aid in making this method a very attractive alternative for large scale printing of selected area gratings.

As we gain experience with this technique, it remains our challenge to critically and thoroughly examine PIC process optimization and yield issues associated with this new selective area grating process.

REFERENCES

1. R.C. Tiberio, G.A. Porkolab, M.J. Rooks, E.D. Wolf, R.J. Lang, A. Larsson, S. Forouhar, J. Cody, G.W. Wicks, T. Erdogan, O.King and D.G. Hall, J. Vac. Sci. Technol B**9**, 2842 (1991).
2. C.E. Zah, C. Caneau, S.G. Menocal, A.S. Godz, P.S.D. Lin, F. Favire, A. Yi-Yan, T.P. Lee, A.G.. Joyner, and C.H. Joyner, Electron. Lett. **25**, 650 (1989)
3. M. Okai, S. Tsuji, N. Chinone, and T. Harada, Appl. Phys. Lett. **55**, 415 (1989).
4. D.M. Tennant, T.L. Koch, P.P. Mulgrew, R.P. Gnall, F. Ostermeyer, and J-M. Verdiell, J. Vac. Sci. Technol. B **10,** 2530 (1992).
5. D. M. Tennant , T.L. Koch, J-M. Verdiell, K. Feder, R.P. Gnall, U. Koren, M.G. Young, B.I. Miller, M.A. Newkirk, B. Tell, J. Vac Sci Technol. **B 11**, 2509 (1993).
6. G Pakulski, R. Moore, C. Maritan, F. Shephard, M. Fallahi, I. Templeton, and G. Champion, Appl. Phys. Lett. **62**, 222 (1993).
7. D. M. Tennant , K.F. Dreyer, K. Feder, R.P. Gnall, T.L. Koch, U. Koren, B.I. Miller, C. Vartuli, M.G. Young, J. Vac Sci Technol.B (to be publ)
8. M.G. Moharam and T.K. Gaylord, J. Opt. Soc Am. **72,** 1385 (1982).
9. M.G. Moharam, *Private Communication*
10. J-M. Verdiell, T.L. Koch, D.M. Tennant, K. Feder, R.P. Gnall, M.G. Young, B.I. Miller, U. Koren, M.A. Newkirk, and B. Tell, Proceedings of the European Conference on Integrated Optics, Neuchatel, Switzerland,1993 (unpublished), p 4.8.
11. U. Koren, B. I. Miller, G. Eisenstein, R. S. Tucker, G. Raybon, and R. J. Capik, Electron. Lett. **24**, pp. 138-140 (1988).
12. J. L. Zilco, L. J. P. Ketelsen, Y. Twu, D. P. Wilt, S.G. Napholtz, J. P. Blaha, K. E. Strege, V. G. Riggs, D. L. Van Haren, S. Y. Leung, P. M. Nitzsche, J. A. Long, C. B. Roxlo, G. Przyblek, J. Lopata, M. W. Focht and L. A. Koszi, IEEE J. Quantum Electron., **QE-25**, pp. 2091-2095 (1989).
13. T. Kjellberg, R. Schatz, J. Lightwave Technol., **10,** 256 (1992).
14. see for example, ZEP 320 Manufacturer's Product Description, Nippon Zeon Co. Ltd., Tokyo, Japan.